J Mater Sci (2022) 57:1947–1961

Energy materials

Controllable preparation of hierarchical porous carbon aerogel from liquefied wood for supercapacitors

Chunfei Lv[1] and Xiaojun Ma[1,*]

[1] College of Light Industry Science and Engineering, Tianjin University of Science & Technology, Tianjin 300222, People's Republic of China

Received: 2 September 2021
Accepted: 15 October 2021
Published online: 3 January 2022

ABSTRACT

Carbon aerogel (LWCA) with hierarchical porous was prepared from phenolated wood by self-assembling and one-step carbonization/activation process, and the pores formation were be controlled by adjusting the content of hexamethylenetetramine (HMTA). The influence of HMTA concentration on the morphological features and final electrochemical properties of LWCA materials were investigated. The characterization and properties of LWCA were investigated by XRD, XPS and N_2 adsorption. The results showed that the doping of HMTA could orientate the hierarchical porous framework of carbon aerogels, and the best carbon aerogels had uniform coral pore structure. The specific surface area and pore volume was as high as $1845 m^2 g^{-1}$ and $1.05 m^3 g^{-1}$, respectively. In addition, the resulting carbon aerogel exhibits excellent electrochemical performance. LWCA exhibited a high specific capacitance of $154.15 Fg^{-1}$ at $0.5 Ag^{-1}$. High capacitance retention (at the current density of $5 Ag^{-1}$, the specific capacitance retention reaches 92.62%) and excellent rate performance (70% capacitance retention at 5A g^{-1}) were possessed. This work provides a simplified technical method to develop biomass base carbon materials with controllable and layered porous for high charge storage capabilities.

Handling Editor: Stephen Eichhorn.

Address correspondence to E-mail: mxj75@tust.edu.cn

https://doi.org/10.1007/s10853-021-06653-z

GRAPHICAL ABSTRACT

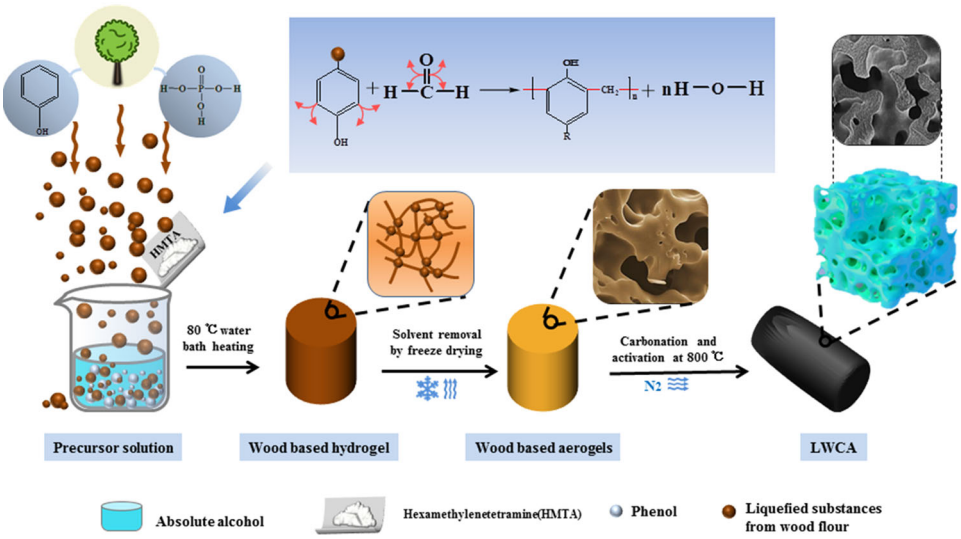

Introduction

With the continuous advancement of the energy transition, the promotion of renewable energy from alternative energy to main energy has attracted the attention of the industry. Electrochemical energy storage occupies an important position in the energy output system, and the development of high-performance energy storage equipment is essential to meet the growing need for small electronic products and modern new energy vehicles [1–3]. Supercapacitors (SCs) have become one of the most promising electrochemical energy storage devices due to their large capacitance [4], ultra-fast charging [5] and discharging process and long cycle life [6]. It can store a large amount of electric charge first, and then release it stably with ultra-high power density. Two charged electrode plates that are very close together will further increase its own capacitance. Undoubtedly, according to the unique energy storage mechanism of supercapacitor, carbon material has become one of the ideal candidate materials for supercapacitor materials by virtue of the advantages of energy storage mechanism of electric double layer capacitor (EDLC) [7, 8].

Recently, various carbon-based materials have been used as commercial supercapacitor electrode materials, such as graphene [9], carbon nanotubes [10], carbon fibers [11], carbon aerogels [12] and carbon nanospheres [13]. Among them, although graphene and carbon nanotubes have high electronic conductivity, large specific surface area and electrochemical stability, the high cost of graphene and carbon nanotubes has limited their wide application [14, 15]. At the same time, the bond interactions of van der Waals force and π-π usually lead to irreversible stacking of graphene nanosheets, which leads to significant reduction of specific surface area and specific capacitance [11, 16]. It is worth noting that carbon aerogels have great research value in energy storage attribute to their low cost, high porosity, large surface area and excellent physical and chemical stability [17, 18]. Phenolic carbon aerogels, as the most traditional carbon aerogels, have been widely studied [19]. Unfortunately, phenols and aldehydes are mainly derived from petrochemical resources, which is widespread concerned because of environmental pollution and unsustainable [20, 21]. Under such circumstances, biomass-based carbon aerogels with controllable carbon structure are of great importance in research as high performance electrochemical materials [22].

Biomass phenol liquefaction is a kind of active liquid substance which is converted from agricultural and forestry biomass resources through liquefaction reaction under the condition of phenol as liquefaction agent [23]. After liquefaction, the liquefied product has thermal fluidity and can be dissolved in some mixed organic solvent binary system, and various polymer materials can be prepared. As a catalyst, acid catalyst can reduce wood components to small components. These components then react with phenol or polyols to form derivatives and dissolve in liquefied solvents. Liquefied products can be used as raw materials for synthetic resins [24]. Compared with traditional carbon aerogels, the preparation of carbon aerogels by wood liquefaction can not only make full use of wood resources at the molecular level, maximize the comprehensive utilization of wood, but also reduce the consumption of petrochemical resources, which is conducive to sustainability.

In the work, we developed a new approach to fabricate biomass-derived carbon aerogel (LWCA) from wood waste by liquefaction, self-assembling and one-step carbonization/activation process. As a traditional catalyst and crosslinking agent, HMTA could promote polycondensation between low molecules and crosslinking between molecular chains. The adjustable network structure and pores formation of LWCA could be controlled by adjusting the content of hexamethylenetetramine (HMTA). The effect of HMTA on the relationship between the microstructure, the surface chemistry and the pore distribution of LWCA was also investigated in detail. Furthermore, electrochemical measurements such as cyclic voltammetry (CV), electrochemical impedance spectroscopy (EIS) and galvanostatic charge/discharge tests were carried out to evaluate the electrochemical properties of LWCA.

Experiments

Materials

Chinese fir (*C. lanceolata*, $0.1 < D < 0.3$ mm) was obtained from the raw Chinese fir debris crushed by the grinder. Phosphoric acid (H_3PO_4), phenol, formaldehyde solution (37.5 wt%) and hexamethylenetetramine (HMTA) were all provided by Damao Chemical Reagent Factory, Tianjin, China. Absolute ethanol was used as a solvent. All chemicals were analytical pure (AR) and used directly during the experiment.

Synthesis of wood-based carbon aerogels from liquefied wood (LWCA)

The liquefied wood was obtained according to the previous studies [25]. The LW gels were prepared by the one-pot sol − gel process. In a typical synthesis, 5 g of liquefied wood (LW) and hexamethylenetetramine (0.9wt% on the weight of LW) was added to 3 ml of absolute ethanol mixed solvent in a glass tube followed by stirring at room temperature to obtain a homogeneous solution. Then, 3 ml of formaldehyde (F) was added to the above solution, and the mixed solution was sonicated for 20 min. The obtained solution was placed into the closed container and kept at 85 °C for 72 h for gelation and aging. The obtained wet gels were subjected to solvent exchange with absolute ethanol followed by freeze-drying process for 10 h at − 60 °C. The obtained aerogels (LWA) were heated in N_2 at 5 °C min^{-1} up to 800 °C for 1 h, and then held isothermally for 1 h under a steam flow of 5 g min^{-1}. Finally, carbon aerogels from liquefied wood (LWCA) were prepared by one-step carbonization/activation process. Various concentrations of HMTA were used to control the pore structure of LWCA, the obtained samples were named with LWA-x and LWCA-x (x = 1, 2, 3, 4, representing 0.9, 1.8, 2.7 and 3.6 wt% of HMTA, respectively).

Characterization

The surface of the sample was tested by scanning electron microscope (SEM, jsm-it300lv), and the microstructure of the sample was obtained. X-ray diffraction (XRD) measurement was taken using an X-ray diffractometer (Ultima IV), where the current and voltage were maintained at 40 mA and 40 kV, respectively, and the wavelength was λ = 1.5418. The crystal structure of the sample was tested from 10° to 80° at a scanning speed of 5° min^{-1}. Raman spectra were obtained by Horiba scientific LabRAM HR evolution spectrometer. The laser excited 532 nm to avoid damaging the sample. The specific surface area and pore size distribution of the samples could be easily obtained by micrometrics Tristar II 3020 instrument test and Brunauere–Emmette–Teller

(BET) model. The specific surface area of micropores was measured by t-plot method. The total pore volume of single point method and micropore volume of t-plot method were used. Before measurement, the sample was degassed with N_2 at 120 °C for 10 h. X-ray photoelectron spectroscopy (XPS) test was performed with Al Kα rays (1486.6 eV) on Thermo Scientific K-Alpha.

Electrochemical measurements

The electrochemical workstation was used to characterize the electrochemical properties of the samples at room temperature. The three electrode system consists of counter electrodes (15 mm × 15 mm platinum electrodes), working electrode (coated nickel foam electrode) and reference electrode (HgO reference electrode). The preparation methods of the working electrodes were as follows: the mixture of active materials, polytetrafluoroethylene (PTFE) and carbon black (mass ratio 8:1:1) was mixed into N-methyl pyrrolidone to form slurry, and then evenly coated on foam nickel sheet (10 mm × 10 mm). It needs to be dried at 80 °C for 12 h before pressing. Electrochemical measurement was taken through CS310H electrochemical workstation (Wuhan Cortest). Constant current charge and discharge test (GCD) (working potential is − 1 to 0 V), cyclic voltammetry (CV) and electrochemical impedance spectroscopy (EIS) were used to study the electrochemical properties of samples. The electrolyte was 6 M KOH solution. With the aid of GCD curve, the weight specific capacitance C of LWCA-x could be obtained by the calculation formula on the following equations:

$$C = (I \times \Delta t)/(m \times \Delta V) \quad (1)$$

where "I" represents the current density, "Δt" represents the discharge time, "m" is the mass of the active substance and finally "ΔV" is the voltage interval without IR drop [26].

Results and discussion

Synthesis and Characterization of LWCA-x

The synthetic pathway of LWCA with self-assembled hierarchical porous coral network structure is illustrated in Fig. 1. Under the catalysis of acid, wood was liquefied by phenol to form phenolic wood, and then reacted with formaldehyde to form macromolecular long chain. Under the action of curing agent (HMTA), a series of crosslinking action took place in the system, and finally formed the gel. The high temperature carbonization of aerogels led to the transformation of carbon skeleton into ordered carbon structure, and the removal of organic matter from the structure significantly increased the conductivity of the material [27]. In addition, after carbonization, the compactness of the material became higher, and the stacking of internal particles became denser, which was more conducive to the conduction of electrons. Moreover, activation was a commonly used method to regulate pore structure of carbon aerogels [28]. The steam one-step activation technology not only reduced the cost and environmental pollution, but also simplified the preparation process to a large extent.

The physical state of the hydrogel prepared from the wood liquefaction will further reflect the influence of the different content of the curing agent on the system. As shown in Fig. 2a, with the increase of curing agent content in the system, the strength of hydrogel gradually increased, which directly verified the generation of different hydrogel structures. In addition, if the system contained excessive curing agent, a large amount of aqueous liquid will be generated during the preparation process, which corresponded to the equation in Fig. 1. The phenomenon in Movie S1 indicated that the residual liquid in the system was spilled after the aerogels were extruded by external forces. After removing the external force, the sample recovered its original morphology, and the spilled liquid returned to the system again. This may be attributed to the regulation of HMTA on the pores of carbon aerogels, which provided a basis for further SEM testing. Figure 2b shows LWCA-x after carbonization activation. Among them, high HMTA content brought about the formation of excessive volatile products in the structure. After high temperature calcination, volatile products escaped, which might be the reason for the excessive volume expansion of LWCA-4.

SEM images showed the morphology of all samples, including aerogels and carbon aerogels (Fig. 3). As can be seen from Fig. 3a, the samples with less curing agent showed a smooth and flat morphology. After carbonization, the structure of LWCA-1 did not change significantly (Fig. 3b). It was worth noting

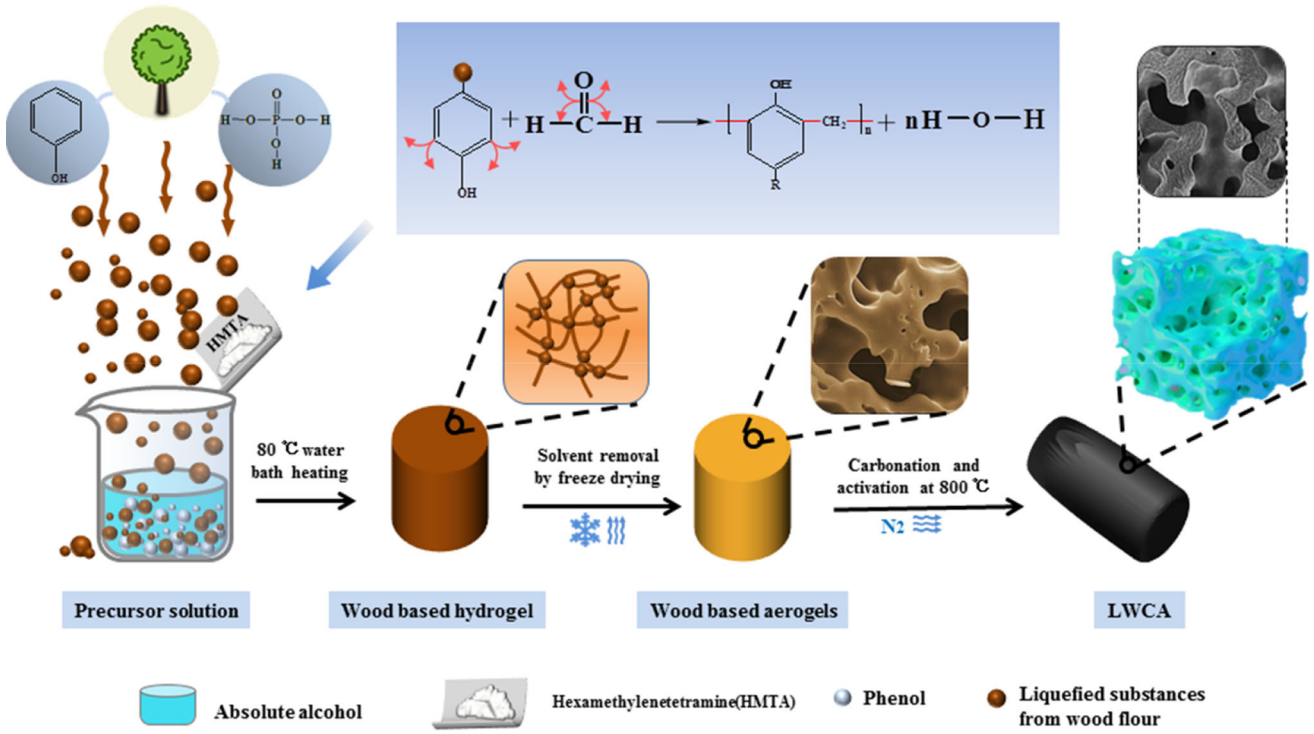

Figure 1 Synthesis route of porous carbon aerogel from wood liquefaction.

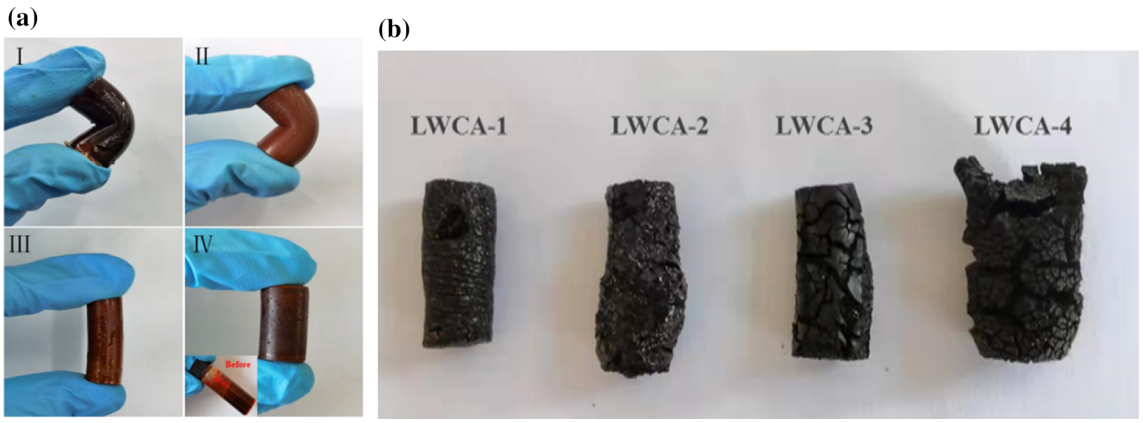

Figure 2 The digital image shows **a** hydrogels with different HMTA content and carbonized **b** HMTA-x.

that the further increase of curing agent content could increase the strength of structural crosslinking, and even led to the formation of obvious pore structure (Fig. 3a, c, e, g). Except for LWCA-4, the original spatial structure of the samples was almost maintained after calcination at high temperature. LWCA-3 had abundant coral-like pore structure. This kind of structure could make the electrolyte easy to enter into the structure, which will shorten the diffusion distance and penetration time of the electrolyte.[29]. Obviously, the coral network structure of the aerogel before carbonization was also helpful for carbonization and water vapor activation. With further increase the ratio of HMTA (Fig. 3h), the carbonized sample showed a large degree of structural collapse. In general, it was confirmed that the addition of MHTA resulted in the formation of a specific interconnected porous network. This was consistent with the macroscopic characterization of Fig. 2. It was fully illustrated that the controllable preparation of layered porous carbon aerogels could be easily realized by controlling the amount of HMTA added.

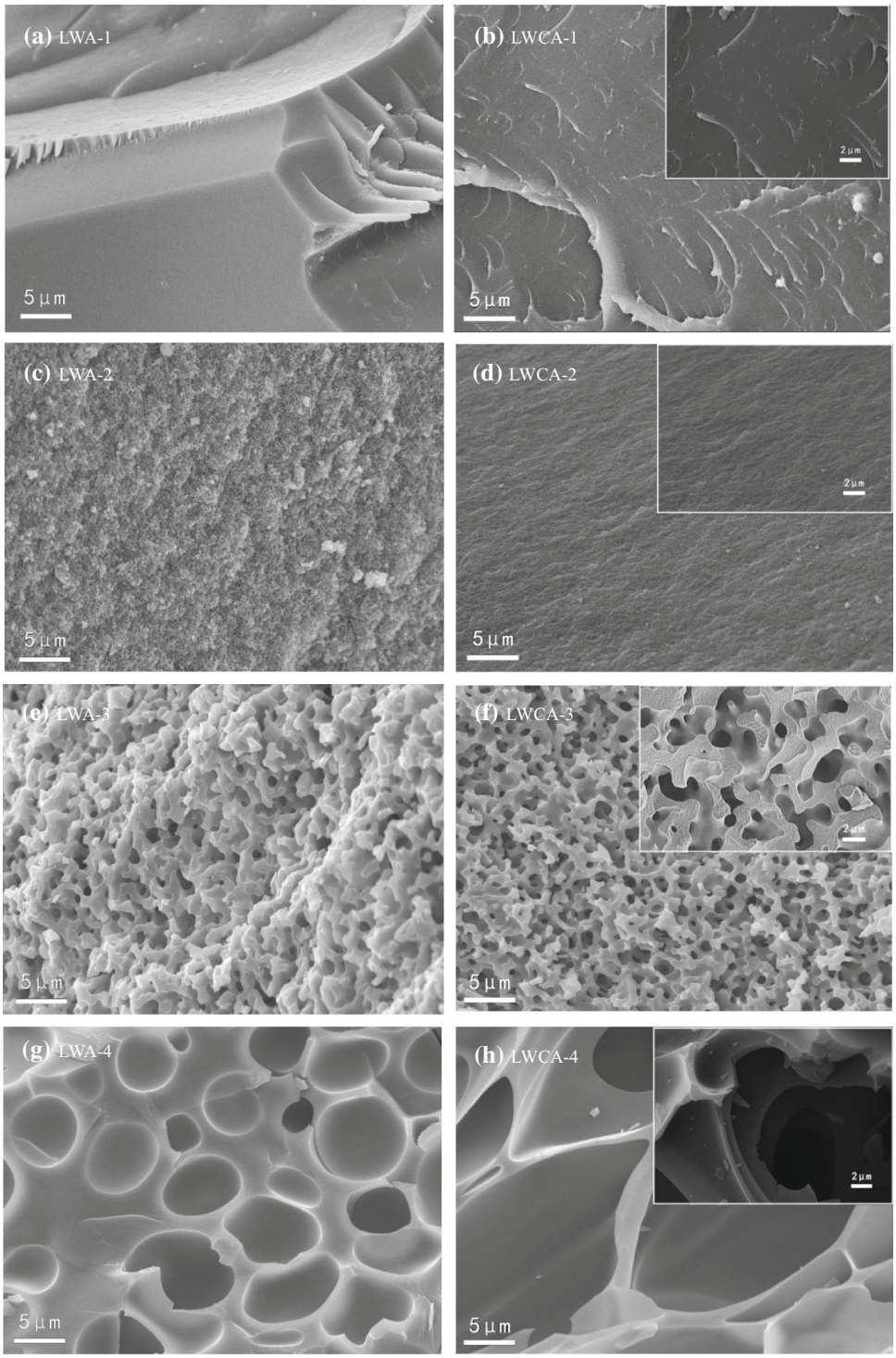

Figure 3 SEM of samples: a, c, e and g were aerogels containing different concentrations of HMTA, b, d, f and h are carbon aerogels containing different concentrations of HMTA.

XRD diffractograms of LWCA-x samples are shown in Fig. 4a. Similar to conventional carbon materials, strong XRD peaks $2\theta = 24$ and 43° were found, which was assigned to the disordered graphitic (002) plane and (100) plane [30]. The pickup position shown in the XRD spectrum in the figure was indexed to the (002) and (100) spacing, which was used to characterize the disordered (amorphous) structure of LWCA-x [31]. With the increase of HMTA content, the diffraction peak shifted. According to Eq. $2d\sin\theta = n\ \lambda$ (d is the plane spacing, n is the interference series, θ is the diffraction

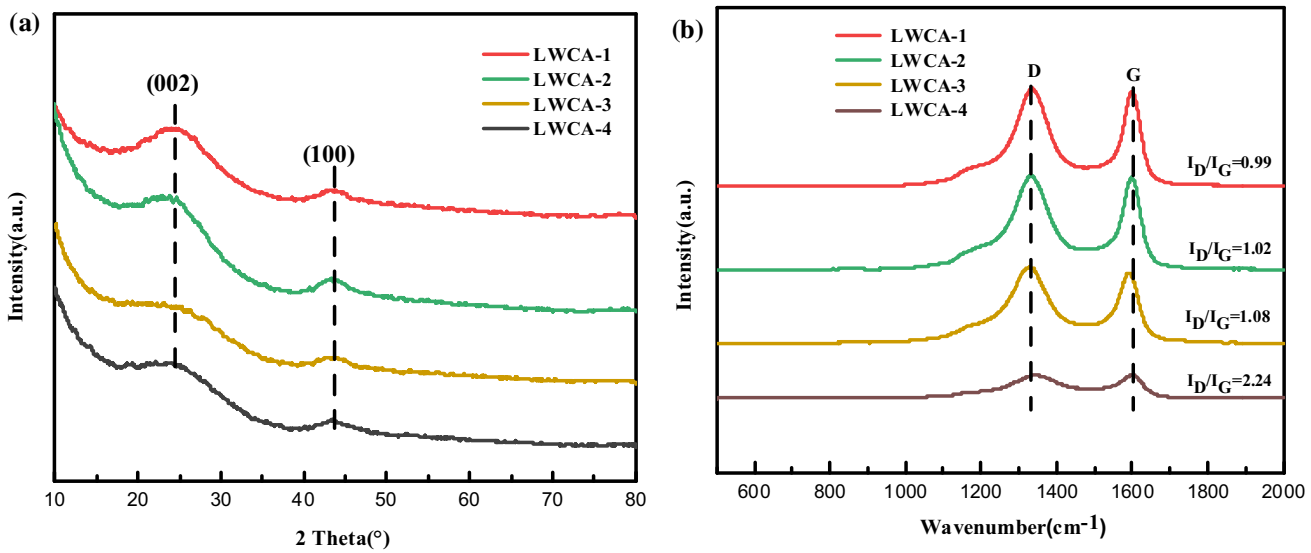

Figure 4 XRD pattern **a** and Raman spectrum **b** of LWCA.

angle, λ is the incident wave length), LWCA-3 had the largest diffraction angle and the smallest crystal plane spacing (for LWCA-1, LWCA-2, LWCA-3 and LWCA-4, the calculated d is 0.36, 0.37, 0.35 and 0.35, respectively). In addition, LWCA-3 had the widest and weakest diffraction peak. This proved that LWCA-3 had the largest number of defects. At the same time, Raman spectroscopy (Fig. 4b) was used to verify the graphitization of the four samples. All samples showed two distinct peaks at ~ 1337 and ~ 1600 cm^{-1}. The two main peaks corresponded to bands D (associated with defect/disordered carbon) and G (band sp2 carbon atoms are generated by in-plane vibration, corresponding to graphite carbon). It was well known that the intensity ratio of the D/G belt (I_D/I_G) was be used to measure the degree of graphitization [21]. For LWCA-1, LWCA-2, LWCA-3 and LWCA-4, the intensity ratio of the D/G band (I_D/I_G) was 0.99, 1.02, 1.08 and 1.04, respectively, indicating that the curing agent content will affect the defects and disorder of the LWCA structure. Among them, the structural defects and disorder of LWCA-3 were higher than that of other samples.

The elemental chemical states on LWCA-x surface were determined by XPS analysis [32]. It could be confirmed that the four samples showed diffraction peaks near the binding energies of 284, 532, 400 and 133 eV, corresponding to C 1 s, O 1 s, N 1 s and P 2p, respectively (Fig. 5a). Among them, the deconvolution C 1 s spectrum of LWCA-3 (Fig. 4b) included four bands of 284.6, 285.0, 286.5 and 289.5 eV, corresponding to different carbon functional groups of C–C, C–N/C–O, C–O and C=O, respectively, which was mainly caused by the intrinsic graphitization structure and surface functional groups [33]. Table 1 shows the contents of carbon, nitrogen, oxygen and phosphorus in LWCA-3. The fitting analysis results of characteristic peaks of N 1 s high-resolution XPS spectrum are shown in Fig. 5c, including three characteristic peaks of pyridine nitrogen (N-6), pyridine (N-5) and quaternary nitrogen/nitrogen oxides (N-Q), corresponding to the binding energies at 398.5, 401 and 402.2 eV, respectively[34]. Studies have shown that N-5 and N-6 contribute to the formation of pseudocapacitance, while N-Q can improve the conductive properties of the material through electron transfer of graphite [4, 22, 35]. To some extent, doping of heteroatoms can make the original carbon aerogel material have more defects and active sites. The O 1 s and P 2p spectra of LWCA-3 (Fig. 5c and Fig. 5d) revealed the presence of O and P elements. Among them, the functionalities containing phosphorus came from the residual phosphoric acid in liquefied wood raw materials. The XPS high-resolution fine patterns of LWCA-1, LWCA-2 and LWCA-4 are shown in Figure S1. Similar to LWCA-3, the other three samples all had similar surface elemental chemical states.

The pore properties of LWCA-x were studied by N_2 adsorption-adsorption isotherm (Fig. 6). The isotherms of all samples after activation showed a

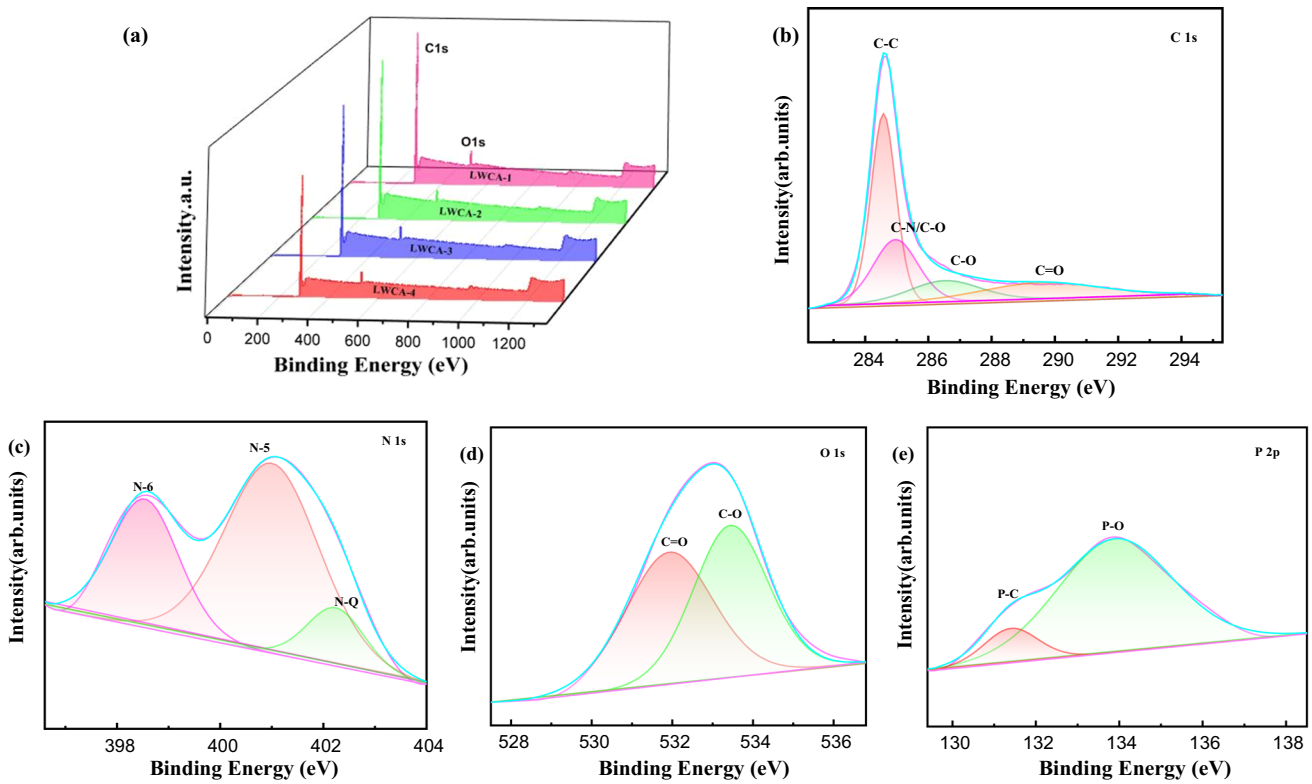

Figure 5 **a** The XPS survey spectrum, **b** C1s spectrum, **c** N1s spectrum, **d** O1s spectrum and **e** P 2p spectrum of LWCA-3.

combined isotherm of type I and type IV (Fig. 6a) [36]. The curve rose rapidly under relatively low pressure ($P/P_0 < 0.05$), and a slight hysteresis loop appeared in the range of $0.4 < P/P_0 < 0.9$, which represented the existence of micropores and mesopores [37]. Figure 6b shows the pore size distribution of LWCA-x. Barrett–Joyner–Halenda (BJH) model was usually used to characterize pore size distribution. The pore size was mainly concentrated in 0.5–4 nm. Table 1 shows the specific surface area and pore volume related parameters of LWCA-x. The average pore diameters of the four samples were all above 2 nm. In addition, the specific surface areas of LWCA-1, LWCA-2 and LWCA-4 were $1186 m^2 g^{-1}$, $1575 m^2 g^{-1}$ and $1538 m^2 g^{-1}$, respectively, while the specific surface area of LWCA-3 was as high as $1845 m^2 g^{-1}$. The specific surface area and pore volume of LWCA-x samples increased first and then decreased with the increase of HMTA content. When HMTA content was 2.7 wt%, the V_{tot} of LWCA-3 reached at 1.05 $cm^3 g^{-1}$. What could be obtained from the information in the table is that the mesopores in the system dominate. These results were caused by the unique pore structure of LWCA-3. From the above analysis, the specific surface and porous structure of LWCA could be controlled by adjusting the content of HMTA. During the activation process, the coral-like structure of LWCA-3 was more conducive to the entry of steam. Therefore, this was one of the reasons why the sample had large specific surface area and reasonable pore size distribution. Obviously, layered porous structure and large specific surface area of LWCA-3 could improve its electrochemical properties. It was beneficial to the rapid diffusion and adsorption of electrolyte ions on the large surface, and mesoporous was beneficial to the ion transport. At the same time, it could make the electrolyte have better permeability between the sample structures. The microporous structure can improve the contact area of the sample. Therefore, LWCA-3 had the most effective electrochemical double layer capacitance performance when applied in supercapacitors [38, 39].

Electrochemical performance

In order to explore the electrochemical performance, LWCA-x was evaluated in a typical three electrode system in a 6 M KOH aqueous electrolyte. Cyclic

Table 1 Porosity parameters and XPS of chemical composition of LWCA-x

Samples	SSA (m^2g^{-1})				Pore volume (cm^3g^{-1})				XPS (at.%)				
	S_{BET}(m^2 g^{-1})	S_{micro}(m^2 g^{-1})	S_{meso}(m^2g^{-1})	S_{micro}/S_{BET} (%)	V_{tot}(cm^3g^{-1})	V_{micro}(cm^3g^{-1})	V_{meso}(cm^3g^{-1})	Dave(nm)	C	O	N	P
LWCA-1	1186	362	824	30.55	0.66	0.18	0.48	2.24	92.58	6	0.96	0.46
LWCA-2	1575	300	1274	19.06	0.97	0.18	0.80	2.48	94.19	5.13	0.54	0.13
LWCA-3	1845	498	1346	27.01	1.05	0.28	0.78	2.25	94.19	4.97	0.66	0.18
LWCA-4	1538	613	925	39.86	0.89	0.34	0.56	2.32	93.33	5.81	0.68	0.18

voltammetry (CV), constant current charge and discharge (GCD) and electrochemical impedance spectroscopy (EIS) were used [40]. Figure 7a shows the CV curves of different electrode materials at a scan rate of $5mVs^{-1}$. The curve of all sample showed an approximate rectangular shape, indicating the excellent electric double layer capacitance response of the electrode material [41]. It was worth noting that the area enclosed by the rectangle corresponded to the maximum and minimum specific capacitance in the CV curve [42]. LWCA-3 had the largest rectangular area, meaning that it had the largest specific capacitance at the same scan rate, which was attributed to the unique framework structure and larger pore volume of LWCA-3. Further, the LWCA-3 sample was tested at a scan rate of 5-$100mVs^{-1}$ (Fig. 7b). It was found that even at a scan rate of $100mVs^{-1}$, the CV curve of the sample still exhibited a perfect approximately rectangular shape without deformation, demonstrating that the combination of mesopores structure and micropores structure of LWCA-3 provided an ion transfer pathway, showing fairly fast electrochemical response and excellent rate stability [43].

Figure 7c shows the GCD curve of all samples at a current density of $0.5Ag^{-1}$. The lines of all samples in the figure were approximately triangular, indicating that the electrochemical response mainly came from the electric double layer and had good electrochemical reversibility [44]. The ohmic drop was negligible, indicating ideal capacitance characteristics with fast I-V response and small resistance [32]. In addition, It could be seen from Fig. 7c that LWCA-3 had the longest charging time and discharging time, revealing that LWCA-3 had the highest specific capacitance under the same current density, which was consistent with Fig. 7a [33]. Figure 7d shows the individual measurements of LWCA-3 at different current densities. The charge–discharge curves of LWCA-3 showed an approximate isosceles triangle shape, and there was no obvious deformation under the condition of 5 A g^{-1}, and exhibited its excellent rate performance and small internal resistance, which was attributed to the large active surface, short diffusion path and good electrical conductivity [45].

Electrochemical impedance spectroscopy (EIS) was used to analyze electrode resistance and electrolyte diffusion resistance. The morphology and structure of materials had great influence on the transport of ions and charges [46]. Figure 7e shows Nyquist plots

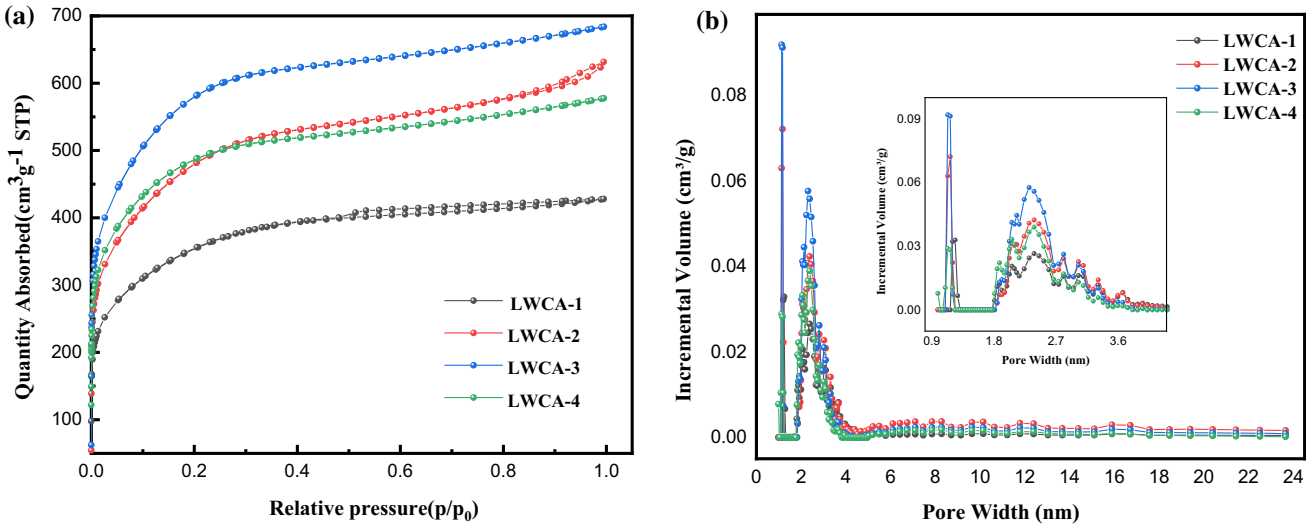

Figure 6 **a** N2 adsorption/desorption isotherms and **b** pore size distributions of LWCA-x.

of samples. As shown in the Fig. 7e, the EIS curves of all samples had smaller ohmic resistance (RS) and very low charge transfer resistance. It was found that the curve of LWCA-3 in the low frequency region was the most vertical and had the shortest 45° transition section, meaning that the resistance of LWCA-3 was smaller than other samples. According to previous analysis, the formation of coral-like macropores and the opening of the pores could greatly increase the contact area between the electrolyte and the carbon material [47]. LWCA-3 had a reasonable layered nanopore structure, which could not only provide more accessible surface products for ions, but also acted as an ion channel to increase the diffusion rate of electrolyte ions [48]. High specific surface area provided abundant storage conditions for charge. LWCA-x showed high utilization rate in electrochemical behavior through controllable preparation scheme and three-dimensional highly interconnected structure [49]. In addition, coral-like structure and large specific surface area were the key to the preparation of carbon electrode materials.

For carbon materials, good capacitance performance needs many factors such as pore structure and conductivity to complete [50]. For carbon aerogel from liquefied wood, the layered porous structure not only completed the efficient transmission of electrolyte ions, but also provided more storage sites for charge (Fig. 7f). As we all know, the capacitance was the key factor for the electrode material [51, 52]. According to formula (1), the specific capacity of LWCA-1, LWCA-2, LWCA-3 and LWCA-4 is 120.03, 132.2, 154.15 and 97.13 Fg^{-1} at the current density of 0.5A g^{-1} in 6 M KOH electrolyte, respectively. In addition, the published data of the specific capacitance of LWCA as a single electrode showed higher values than other carbon materials in the current work mentioned in Table 2. The breakthrough advantage of LWCA-3 was due to its high specific surface area and a large number of mesoporous structures. As we all know, after carbonization at a certain temperature (generally higher than 650 °C), the amorphous carbon formed in the carbon framework at low temperature transforms into an ordered carbon structure of sp2, which significantly improved the conductivity of the LWCA-3 material. The specific capacitance of aerogel had a certain degree of contribution [27]. Under the same conditions, after the current density was increased by ten times, the capacitance retention rate reached more than 70%, which proved the excellent rate capability of LWCA-3 (Fig. 8a). As shown in Fig. 8b, the GCD experiment was carried out at a current density of $5Ag^{-1}$. After 4500 cycles, the weight specific capacitance of LWCA-3 electrode material did not decrease significantly. The cyclic stability of the material was maintained at 92.62%. Moreover, the GCD curves of the first cycle and the last cycle overlap well, which proved that the electrode material has no obvious change after multiple charge and discharge, and had good cycle stability.

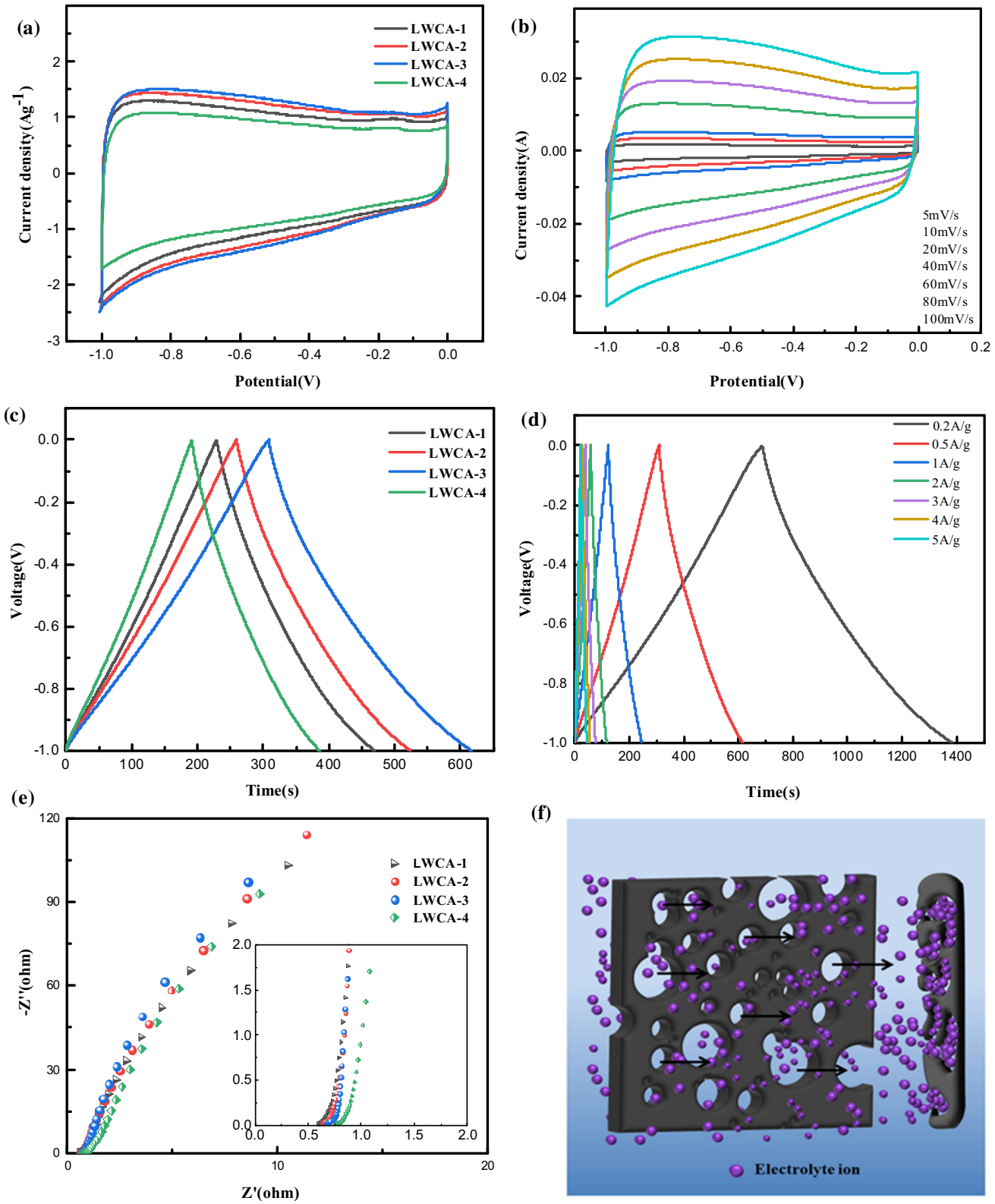

Figure 7 **a** CV curves of LWCA-x at 10mVs^{-1}, **b** CV curves of LWCA-x at different scanning rates, **c** GCD curves of LWCA-3 sample, **d** GCD curves of at different current densities, **e** Nyquist plots of samples and **f** schematic diagram of electrolyte ion storage.

Table 2 The comparison of the specific capacitance of carbon materials

Electrode materials	Raw materials	SSA (m^2 $g^{-1)}$	Capacitance (F g^{-1})	Testing conditions	Reference
aCA	CMC	428	152.6	0.5 A g^{-1}, 6 M KOH	[12]
S-CA	Phenols, aldehydes	830	105	1 A g^{-1}, 6 M KOH	[26]
NGAs	Melamine, GO	157	170.5	0.2 A g^{-1}, 6 M KOH	[53]
CA-L20	Lignin, R, F	779	142.8	0.5 A g^{-1}, 6 M KOH	[54]
OM-CA	H2O2, phenols, aldehydes	450	151	0.5 A g^{-1}, 6 M KOH	[55]
CAs	Starch, phenols and aldehydes	734	147	1 A g^{-1}, 6 M KOH	[44]
rGO(180) aerogel	GO,CNT	-	129	0.1 A g^{-1}, 1 M Na_2SO_4	[56]
LWCA	Chinese fir, phenol, formaldehyde solution	1845	154.15	0.5 A g^{-1}, 6 M KOH	This work

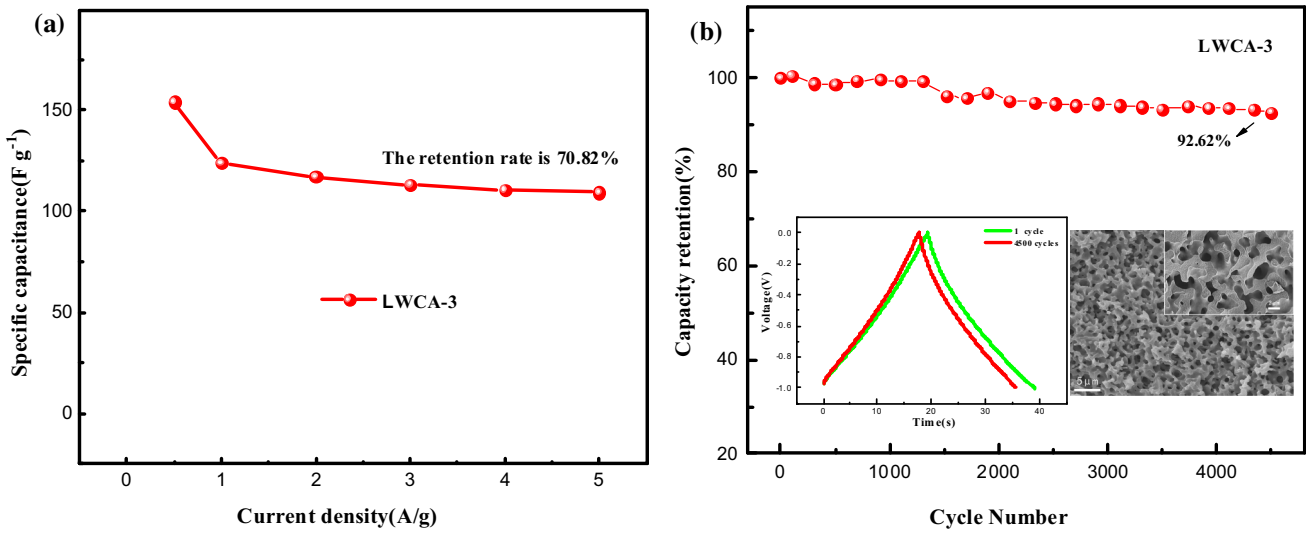

Figure 8 Specific capacitance retention **a** and cycle life **b** of LWCA-3.

Conclusion

A hierarchical porous carbon aerogel with controllable structure was prepared by using wood liquefaction, followed by steam activation. Benefit from low density, controllable pore size and large specific surface area, the electrode prepared by this material as the preparation of supercapacitor showed very good electrochemical performance. Among them, hexamethylenetetramine (HMTA) was used as the structural control agent to prepare LWCA-x (x = 1,2,3,4, respectively). The final results showed that the specific surface area of the samples were as high as 1845m^2g^{-1} in the three electrode system with current density of 0.5Ag^{-1}. LWCA-3 had a high specific capacitance of 154.15Fg^{-1}. Even if the current density was increased ten times, the retention rate of specific capacitance was still above 70%. LWCA-3 had a wide range of pore structure and high stability, which was conducive to the further study of supercapacitor electrode materials. In addition, extraction of wood rich carbon aerogels from rich biomass materials played a key role in exploring economically sustainable biomass materials.

Acknowledgements

This work was supported by the National Natural Science Foundation of China (No. 31870564).

Declarations

Conflict of interest No conflict of interest exits in the submission of this manuscript, and manuscript is approved by all authors for publication.

Supplementary Information: The online version contains supplementary material available at https://doi.org/10.1007/s10853-021-06653-z.

References

[1] Tian WW, Cheng DK, Wang S, Xiong CX, Yang QL (2019) Phytic acid modified manganese dioxide/graphene composite aerogel as high-performance electrode materials for supercapacitors. Appl Sur Sci 495:143589. https://doi.org/10.1016/j.apsusc.2019.143589

[2] Yin QW, He LW, Lian JQ, Sun JJ, Xiao SF, Luo JJ, Sun DY, Xie A, Lin BZ (2019) The synthesis of Co_3O_4/C composite with aloe juice as the carbon aerogel substrate for asymmetric supercapacitors. Carbon 155:147–154. https://doi.org/10.1016/j.carbon.2019.08.060

[3] Lei E, Li W, Sun JM, Wu ZW, Liu SX (2019) N-doped carbon aerogels obtained from APMP fiber aerogels saturated with rhodamine dye and their application as supercapacitor electrodes. Appl Sci 9:618. https://doi.org/10.3390/app9040618

[4] Khammar H, Abdelwahab A, Abdel-Samad HS, Hassan HH (2020) Synergistic performance of simply fabricated polyaniline/carbon xerogel composite as supercapacitor electrode. J Electroanal Chem 880:114848. https://doi.org/10.1016/j.jelechem.2020.114848

[5] Zhuo H, Hu YJ, Chen ZH, Zhong LX (2019) Cellulose carbon aerogel/PPy composites for high-performance supercapacitor. Carbohydr Polym 215:322–329. https://doi.org/10.1016/j.carbpol.2019.03.101

[6] Zhang XF, Li H, Zhang W, Huang ZJ, Tsui CP, Lu CH, He CG, Yang YK (2019) In-situ growth of polypyrrole onto bamboo cellulose-derived compressible carbon aerogels for high performance supercapacitors. Electrochim Acta 301:55–62. https://doi.org/10.1016/j.electacta.2019.01.166

[7] Raj CJ, Manikandan R, Rajesh M, Sivakumar P, Jung H, Das SJ, Kim BC (2021) Cornhusk mesoporous activated carbon electrodes and seawater electrolyte: the sustainable sources for assembling retainable supercapacitor module. J Power Sources 490:229518. https://doi.org/10.1016/j.jpowsour.2021.229518

[8] Liu YH, Zhang XF, Gu X, Wu NX, Zhang RN, Shen Y, Zheng B, Wu JS, Zhang WN, Li S, Huo FW (2020) One-step turning leather wastes into heteroatom doped carbon aerogel for performance enhanced capacitive deionization. Microporous Mesoporous Mater 303:110303. https://doi.org/10.1016/j.micromeso.2020.110303

[9] Yang QL, Yang JW, Gao ZDF, Li B, Xiong CX (2019) Carbonized cellulose nanofibril/graphene oxide composite aerogels for high-Performance supercapacitors. ACS Appl Energy Mater 3:1145–1151. https://doi.org/10.1021/acsaem.9b02195

[10] Liu YF, Chang XY, Wang MY, Guo HN, Li WQ, Wang YJ (2021) Hierarchical $CuCo_2O_4$/CuO nanoflowers crosslinked with carbon nanotubes as an advanced electrode for supercapacitors. J Alloys and Compd 871:159555. https://doi.org/10.1016/j.jallcom.2021.159555

[11] Liu X, Zang LM, Xu YJ, Liu QF, You H, Chen MZ, Yang C (2021) Activated carbon fiber yarns with birnessite-type MnO_2 and oxygen-functional groups for high-performance flexible asymmetric supercapacitors. Diamond Relat Mater 115:108371. https://doi.org/10.1016/j.diamond.2021.108371

[12] Yu M, Li J, Wang LJ (2017) KOH-activated carbon aerogels derived from sodium carboxymethyl cellulose for high-performance supercapacitors and dye adsorption. Chem Eng J 310:300–306. https://doi.org/10.1016/j.cej.2016.10.121

[13] Zheng LP, Dai XC, Ouyang YH, Chen YL, Wang XY (2021) Highly N/O co-doped carbon nanospheres for symmetric supercapacitors application with high specific energy. J Energy Storage 33:102152. https://doi.org/10.1016/j.est.2020.102152

[14] Lu ZW, Xu XC, Chen YJ, Wang XH, Sun L, Zhuo KL (2020) Nitrogen and sulfur co-doped graphene aerogel with hierarchically porous structure for high-performance supercapacitors. Green Energy Environ 5:69–75. https://doi.org/10.1016/j.gee.2019.06.001

[15] Chen YJ, Jiang YY, Liu ZE, Yang LF, Du QZ, Zhuo KL (2020) Hierarchical porous N-doped graphene aerogel with good wettability for high-performance ionic liquid-based supercapacitors. Electrochim Acta 366:137414. https://doi.org/10.1016/j.electacta.2020.137414

[16] Cheng C, Li D (2013) Solvated graphenes: an emerging class of functional soft materials. Adv Mater 25:13–30. https://doi.org/10.1002/adma.201203567

[17] Ibarra Torres CE, Serrano Quezada TE, Kharissova OV, Kharisov BI, Gómez de la Fuente MI (2021) Carbon-based aerogels and xerogels: synthesis, properties, oil sorption capacities, and DFT simulations. J Environ Chem Eng 9:104886. https://doi.org/10.1016/j.jece.2020.104886

[18] Abbas Q, Raza R, Shabbir I, Olabi AG (2019) Heteroatom doped high porosity carbon nanomaterials as electrodes for energy storage in electrochemical capacitors: a review. J Sci:

Adv Mater Devices 4:341–352. https://doi.org/10.1016/j.jsamd.2019.07.007

[19] Pekala RW (1989) Organic aerogels from the polycondensation of resorcinol with formaldehyde. J Mater Sci 24:3221–3227. https://doi.org/10.1007/BF01139044

[20] Liu HL, Wang P, Zhang B, Li HY, Li J, Li YJ, Chen Z (2021) Enhanced thermal shrinkage behavior of phenolic-derived carbon aerogel-reinforced by HNTs with superior compressive strength performance. Ceram Int 47:6487–6495. https://doi.org/10.1016/j.ceramint.2020.10.232

[21] Ma Y, Yin JW, Liang HQ, Yao DX, Xia YF, Zuo KH, Zeng Y-P (2021) A two step approach for making super capacitors from waste wood. J Cleaner Prod 279:123786. https://doi.org/10.1016/j.jclepro.2020.123786

[22] Sun JM, Li W, Lei E, Xu Z, Ma CH, Wu ZW, Liu SX (2019) Ultralight carbon aerogel with tubular structures and N-containing sandwich-like wall from kapok fibers for supercapacitor electrode materials. J Power Sources 438:227030. https://doi.org/10.1016/j.jpowsour.2019.227030

[23] Deshavath NN, Goud VV, Veeranki VD (2021) Liquefaction of lignocellulosic biomass through biochemical conversion pathway: a strategic approach to achieve an industrial titer of bioethanol. Fuel 287:119545. https://doi.org/10.1016/j.fuel.2020.119545

[24] Lee WJ, Chen YC (2008) Novolak PF resins prepared from phenol liquefied cryptomeria japonica and used in manufacturing moldings. Bioresour Technol 99:7247–7254. https://doi.org/10.1016/j.biortech.2007.12.060

[25] Wang LN, Ma XJ (2020) Preparation of N, P self-doped activated carbon hollow fibers derived from liquefied wood. Wood Sci Technol 55:83–93. https://doi.org/10.1007/s00226-020-01244-8

[26] Zhai ZZ, Ren B, Xu YL, Wang SS, Zhang LH, Liu ZF (2021) Nitrogen self-doped carbon aerogels from chitin for supercapacitors. J Power Sources 481:228976. https://doi.org/10.1016/j.jpowsour.2020.228976

[27] Rhim Y-R, Zhang D, Rooney M, Nagle DC, Fairbrother DH, Herman C, Drewry DG (2010) Changes in the thermophysical properties of microcrystalline cellulose as function of carbonization temperature. Carbon 48:31–40. https://doi.org/10.1016/j.carbon.2009.07.048

[28] Yang X, Kong LY, Ma JF, Liu XG (2018) Facile construction of hierarchically porous carbon nanofiber aerogel for high-performance supercapacitor. J Appl Electrochem 49:241–250. https://doi.org/10.1007/s10800-018-1270-7

[29] He TS, Li XY, Wang YF, Bai TJ, Weng X, Zhang B (2020) Carbon nano-fibers/ribbons with meso/macro pores structures for supercapacitor. J Electroanal Chem 878:114597. https://doi.org/10.1016/j.jelechem.2020.114597

[30] Lee SP, Ali GAM, Hegazy HH, Lim HN, Chong KF (2021) Optimizing reduced graphene oxide aerogel for a supercapacitor. Energy Fuels 35:4559–4569. https://doi.org/10.1021/acs.energyfuels.0c04126

[31] Zhuo H, Hu YJ, Tong X, Zhong LX, Peng XW, Sun RC (2016) Sustainable hierarchical porous carbon aerogel from cellulose for high-performance supercapacitor and CO_2 capture. Ind Crops Prod 87:229–235. https://doi.org/10.1016/j.indcrop.2016.04.041

[32] Pinto SC, Goncalves G, Sandoval S, Lopez-Periago AM, Borras A, Domingo C, Tobias G, Duarte I, Vicente R, Marques P (2020) Bacterial cellulose/graphene oxide aerogels with enhanced dimensional and thermal stability. Carbohydr Polym 230:115598. https://doi.org/10.1016/j.carbpol.2019.115598

[33] Hao P, Zhao ZH, Leng YH, Tian J, Sang YH, Boughton RI, Wong CP, Liu H, Yang B (2015) Graphene-based nitrogen self-doped hierarchical porous carbon aerogels derived from chitosan for high performance supercapacitors. Nano Energy 15:9–23. https://doi.org/10.1016/j.nanoen.2015.02.035

[34] Inagaki M, Toyoda M, Soneda Y, Morishita T (2018) Nitrogen-doped carbon materials. Carbon 132:104–140. https://doi.org/10.1016/j.carbon.2018.02.024

[35] Ma Y, Wu DL, Wang T, Jia DZ (2019) Nitrogen, phosphorus co-doped carbon obtained from amino acid based resin xerogel as efficient electrode for supercapacitor. ACS Appl Energy Mater 3:957–969. https://doi.org/10.1021/acsaem.9b02032

[36] Chen H, Liu T, Mou JR, Zhang WJ, Jiang ZJ, Liu J, Huang JL, Liu ML (2019) Free-standing N-self-doped carbon nanofiber aerogels for high-performance all-solid-state supercapacitors. Nano Energy 63:103836. https://doi.org/10.1016/j.nanoen.2019.06.032

[37] Mirzaeian M, Abbas Q, Gibson D, Mazur M (2019) Effect of nitrogen doping on the electrochemical performance of resorcinol-formaldehyde based carbon aerogels as electrode material for supercapacitor applications. Energy 173:809–819. https://doi.org/10.1016/j.energy.2019.02.108

[38] Zhu XX, Huang XH, Anwer S, Wang NY, Zhang LD (2020) Nitrogen-doped porous carbon nanospheres activated under low $ZnCl_2$ aqueous system: An electrode for supercapacitor applications. Langmuir 36:9284–9290. https://doi.org/10.1021/acs.langmuir.0c01670

[39] Mohamed AM, Abo El Naga AO, Zaki T, Hassan HB, Allam NK (2020) Bimetallic Co–W–S chalcogenides confined in N, S-codoped porous carbon matrix derived from metal–organic frameworks for highly stable electrochemical

supercapacitors. ACS Appl Energy Mater 3:8064–8074. https://doi.org/10.1021/acsaem.0c01513

[40] Ma CX, Wang RX, Tetik H, Gao SJ, Wu M, Tang ZY, Lin D, Ding D, Wu WZ (2019) Hybrid nanomanufacturing of mixed-dimensional manganese oxide/graphene aerogel macroporous hierarchy for ultralight efficient supercapacitor electrodes in self-powered ubiquitous nanosystems. Nano Energy 66:104124. https://doi.org/10.1016/j.nanoen.2019.104124

[41] Zhang Z, Li L, Qing Y, Lu XH, Wu YQ, Yan N, Yang W (2018) Hierarchically interconnected N-doped carbon aerogels derived from cellulose nanofibrils as high performance and stable electrodes for supercapacitors. J Phys Chem C 122:23852–23860. https://doi.org/10.1021/acs.jpcc.8b06550

[42] Zhang HM, Feng JZ, Li LJ, Jiang YG, Feng J (2019) Controlling the microstructure of resorcinol–furfural aerogels and derived carbon aerogels via the salt templating approach. RSC Adv 9:5967–5977. https://doi.org/10.1039/c9ra00238c

[43] Guo J, Wu DL, Wang T, Ma Y (2019) P-doped hierarchical porous carbon aerogels derived from phenolic resins for high performance supercapacitor. Appl Surf Scie 475:56–66. https://doi.org/10.1016/j.apsusc.2018.12.095

[44] Xu YL, Ren B, Wang SS, Dong XX, Zhang LH, Liu ZF (2019) Carbon aerogels with oxygen-containing surface groups for use in supercapacitors. Solid State Ionics 339:115005. https://doi.org/10.1016/j.ssi.2019.115005

[45] Lv ZZ, Li XL, Chen XJ, Li X, Wu M, Li ZG (2019) One-step site-specific activation approach for preparation of hierarchical porous carbon materials with high electrochemical performance. ACS Appl Energy Mater 2:8767–8782. https://doi.org/10.1021/acsaem.9b01729

[46] Li F, Xie LJ, Sun GH, Kong QQ, Su FY, Cao YF, Wei JC, Ahmad A, Guo XY, Chen C-M (2019) Resorcinol-formaldehyde based carbon aerogel: preparation, structure and applications in energy storage devices. Microporous Mesoporous Mater 279:293–315. https://doi.org/10.1016/j.micromeso.2018.12.007

[47] Zhang YF, Zuo LZ, Zhang LS, Yan JJ, Lu HY, Fan W, Liu TX (2016) Immobilization of NiS nanoparticles on N-doped carbon fiber aerogels as advanced electrode materials for supercapacitors. Nano Res 9:2747–2759. https://doi.org/10.1007/s12274-016-1163-1

[48] Yang X, Fei BH, Ma JF, Liu XG, Yang SM, Tian GL, Jiang ZH (2018) Porous nanoplatelets wrapped carbon aerogels by pyrolysis of regenerated bamboo cellulose aerogels as supercapacitor electrodes. J Carbohydr Polym 180:385–392. https://doi.org/10.1016/j.carbpol.2017.10.013

[49] Zhai ZZ, Zheng YX, Du TM, Tian ZS, Ren B, Xu YL, Wang SS, Zhang LH, Liu ZF (2021) Green and sustainable carbon aerogels from starch for supercapacitors and oil-water separation. Ceram Int. https://doi.org/10.1016/j.ceramint.2021.04.229

[50] Lei E, Sun JM, Gan WT, Wu ZW, Xu Z, Xu LF, Ma CH, Li W, Liu SX (2021) N-doped cellulose-based carbon aerogels with a honeycomb-like structure for high-performance supercapacitors. J Energy Storage 38:102414. https://doi.org/10.1016/j.est.2021.102414

[51] Yang XX, Zou HL, Zhang P, Ding H, Ji YH, Li TT, Wei JS, Wei XJ (2020) In-situ self-assembly host-guest carbon aerogels for robust electrochemical capacitors. Electrochim Acta 364:137285. https://doi.org/10.1016/j.electacta.2020.137285

[52] Vijayan BL, Mohd Zain NK, Misnon II, Reddy MV, Adams S, Yang C-C, Anilkumar GM, Jose R (2020) Void space control in porous carbon for high-density supercapacitive charge storage. Energy Fuels 34:5072–5083. https://doi.org/10.1021/acs.energyfuels.0c00737

[53] Xu YL, Wang SS, Yan MF, Zhang LH, Liu ZF (2018) Synthesis, characterization and electrochemical properties of S-doped carbon aerogels. Solid State Ionics 321:91–97. https://doi.org/10.1016/j.ssi.2018.04.009

[54] Xing L-B, Hou S-F, Zhou J, Zhang J-L, Si WJ, Dong YH, Zhuo SP (2015) Three dimensional nitrogen-doped graphene aerogels functionalized with melamine for multifunctional applications in supercapacitors and adsorption. J Solid State Chem 230:224–232. https://doi.org/10.1016/j.jssc.2015.07.009

[55] Xu YL, Ren B, Wang SS, Zhang LH, Liu ZF (2018) Carbon aerogel-based supercapacitors modified by hummers oxidation method. J Colloid Interface Sci 527:25–32. https://doi.org/10.1016/j.jcis.2018.04.108

[56] Okhay O, Tkach A, Gallo MJH, Otero-Irurueta G, Mikhalev S, Staiti P, Lufrano F (2020) Energy storage of supercapacitor electrodes on carbon cloth enhanced by graphene oxide aerogel reducing conditions. J Energy Storage 32:101839. https://doi.org/10.1016/j.est.2020.101839